Performance of Unmanned Aircrafts in the Event of Loss-of-control

Torbjørn Cunis* and Elgiz Baskaya†
French Civil Aviation School, 31055 Toulouse, France

Abstract

Loss of control is a severe and immediate consequence of faults in an unmanned aircraft system during flight. Without recovery, detection of admissible landing spots is necessary to avoid causalities. This case study considers exemplary the MAKO unmanned aircraft and discusses viable trim conditions for a drone system after faults of propulsion and elevator using continuation analysis. Furthermore, simple estimates of reachable zones for controlled flight into terrain are provided.

1 Introduction

As the variety of drone application widens and stakeholder push for further utilisation of the airspace, aviation authorities are busy today with new regulations for unmanned aircraft systems. in order to set a common ground for European aviation and integrate drones safely into the airspace. Due to both decreased cost and accuracy, drone systems are often susceptible to faults of different nature. To achieve a safe integration into the airspace, the problem of detecting anomalies during flight has to be addressed. Taking advantage of intelligent software which processes available information as efficient as possible could serve as an effective way to contribute to the solution of this challenging problem.

Aircraft *loss of control* (LOC) is considered as one of the biggest contributors to fatal accidents. The Joint Safety Analysis Team (JSAT) defines LOC as a "significant, unintended departure of the aircraft from controlled flight, the operational flight envelope, or usual flight attitudes, including ground events" [1], where *significant* refers to events resulting with an incidence or accident. Control failures, inappropriate pilot action (or simply inaction) in a healthy aircraft, and vehicle impairment are examples of LOC events [2]. In-flight loss of control (LOC-I) in particular is the most deadly accident type with 37 fatal accidents per year[1] [3]. Although LOC-I is the cause behind many fatal accidents, manned aviation has a very limited use of LOC prevention and recovery [4]. Having no single action to prevent LOC events, technical limits in LOC simulations such as full stall or failure simulations, constitute some of the challenges on the way to LOC event prevention and recovery solutions. LOC events have been categorized by [5] under five main topics, the most common being aerodynamic stall and flight control system failures. The category of flight control failures, the second most fatal cause of LOC in 15 years log, includes autopilot commands and control surface failures [5]. The study further shows that the percentage of flight control system upset incidents among the other LOC events has risen from 9 % to 22 % after 1993 (pre-1993 compared to 1993–2007). With increased complexity of onboard systems, addressing onboard fault detection and recovery could contribute to reduce the likelihood of LOC accidents and their fatalities.

Designing recovery measures for unmanned systems has further challenges due to the lack of redundancies and use of cheaper and less accurate components compared to manned aviation. Here, fault tolerant control systems (FTCS) are designed to issue solutions to systems which are under fault/failure. There are a wide range of different strategies offered for this solution such as passive or active FTCS, where the latter requires a fault detection and diagnosis (FDD) phase [6]. After the fault is known, the severity of the situation and current abilities of the drone need to be evaluated to decide if a recovery is possible. Recent studies considered viable trim conditions [7, 8], recoverability [9], and control invariant sets [10, 11] of transport aircrafts in case of impairment, reduced efficiency due to icing, or reduced control authority. In case a recovery is likely to fail, a safe ditch manoeuvre can abruptly decrease the number of fatalities. Maps pointing zones with no or minimum population could be uploaded onboard and the safest region to ditch can be selected. Since those situations are usually handled by aircraft pilots assessment and planning of ditch manoeuvres is imperative for the development of unmanned systems. NASA offers *Safe2Ditch* [12] to offer autonomous crash management yet is at design stage now.

In this paper, we provide a case study for discussion of abilities of a drone under failure. We consider an already detected fault of a single control input of the longitudinal aerodynamics – rather than a gradually degradation or impairment of a surface – namely loss of propulsion, loss of elevator, and loss of single aileron, and assess the remaining abilities of the drone including the calculation of possible landing zones in the first two cases.

*Doctoral researcher, ONERA – The French Aerospace Lab, Department of Information Processing and Systems; associated researcher with the French Civil Aviation School, Drones Research Group; e-mail: torbjoern.cunis@onera.fr

†Doctoral researcher, French Civil Aviation School, Drones Research Group; e-mail: elgiz.baskaya@enac.fr

[1] for fixed-wings.

2 MAKO Unmanned Aircraft

The MAKO unmanned aircraft shown in Fig. 1 has been selected as the drone to be modeled in the course of this study. MAKO has an off-the-shelf frame and is equipped with a single, back-facing propeller and two vertical control surfaces. Elevator and aileron of MAKO are combined in a single horizontal surface on each wing, called *elevon*. The frame is designed to be lightweight and easy to repair, and for that reason made from Elapor foam which however is limiting for the structural strength. The specifications of the airframe are given in Tab. 1. Stability derivatives for the aerodynamic forces and moments has been calculated via AVL and given in the appendix (Table 2). AVL is an open source program developed at MIT and uses vortex-lattice method for the aerodynamic and stability calculations. The output of the program is linearised at a selected condition, therefore all the coefficients are calculated around the equilibrium point at 14 m/s cruise flight condition. The centre of gravity is located at $x_{\mathrm{CG}} = 0.295\,\mathrm{m}$, which corresponds to a 8 % positive static margin evaluatated in flight.

Table 1: Parameters of the MAKO aircraft [13].

flight mass	m	0.7–2.0	kg
wing span	b	1.29	m
mean chord	c_A	0.21	m
wing area	S	0.27	m^2
propeller diameter	D	22.8	cm
air density	ϱ	1.27	$\mathrm{kg/m}$
gravitational constant	g	9.81	$\mathrm{m/s}^2$

3 Nonlinear Model

We refer to the axis systems of the international standard: the *body axis system* aligned with fuselage; the *air-path axis system* aligned with the air-path velocity vector $\mathbf{V}_{\mathrm{A}}$; and the *normal earth-fixed axis system*. [14]

3.1 Equations of motion

Consider the ordinary differential equations

$$\dot{\mathbf{x}} = \mathbf{f}(\mathbf{x}, \mathbf{u}) \tag{1}$$

with the state vector $\mathbf{x} = \begin{bmatrix} V_{\mathrm{A}} & \gamma_{\mathrm{A}} & q & \Theta \end{bmatrix}^T$ with airspeed V_{A}, inclination γ_{A}, pitch rate q, and pitch angle Θ; and the inputs $\mathbf{u} = \begin{bmatrix} \eta & n \end{bmatrix}^T$ comprised of elevator deflection η and engine speed n. The nonlinear equations of motion are given with respect to the states as

$$m\dot{V}_{\mathrm{A}} = F\cos\alpha - \frac{1}{2}\varrho V_{\mathrm{A}}^2 S C_{\mathrm{D}}(\alpha, q, \eta) + mg\sin\gamma_{\mathrm{A}}; \tag{2}$$

$$mV_{\mathrm{A}}\dot{\gamma} = F\sin\alpha + \frac{1}{2}\varrho V_{\mathrm{A}}^2 S C_{\mathrm{L}}(\alpha, q, \eta) - mg\sin\gamma_{\mathrm{A}}; \tag{3}$$

$$I_y\dot{q} = \frac{1}{2}\varrho V_{\mathrm{A}}^2 S c_{\mathrm{A}} C_{\mathrm{m}}(\alpha, q, \eta)\,; \tag{4}$$

$$\dot{\Theta} = q; \tag{5}$$

Figure 1: Photograph of the MAKO unmanned aircraft.

and the angle of attack $\alpha = \Theta - \gamma$, where C_{L}, C_{D}, and C_{m} denote the aerodynamic lift, drag, and pitch-moment coefficients, respectively. The thrust force is modeled as function of engine speed and airspeed,

$$F(n) = \varrho n^2 D^4 \left(C_{\mathrm{F0}} + C_{\mathrm{F}J}\frac{V_{\mathrm{A}}}{nD} + C_{\mathrm{F}n} n \right). \tag{6}$$

3.2 Aerodynamic coefficients

Using AVL, we obtain the aerodynamic coefficients for small angles of attack:

$$C_{\mathrm{L}} = C_{\mathrm{L0}} + C_{\mathrm{L}\alpha}\alpha + C_{\mathrm{L}q}\hat{q} + C_{\mathrm{L}\eta}\eta; \tag{7}$$

$$C_{\mathrm{D}} = C_{\mathrm{D0}} + C_{\mathrm{DL}} C_{\mathrm{L}}^2(\alpha, \hat{q}, \eta)\,; \tag{8}$$

$$C_{\mathrm{m}} = C_{\mathrm{m0}} + C_{\mathrm{m}\alpha}\alpha + C_{\mathrm{m}q}\hat{q} + C_{\mathrm{m}\eta}\eta; \tag{9}$$

with the normalized pitch rate $\hat{q} = c_{\mathrm{A}} q / V_{\mathrm{A}}$. We further identified the stall angle of attack in an AVL subroutine [15] to

$$\alpha_{\mathrm{stall}} = 11.3^\circ$$

and extend (7) to

$$C'_{\mathrm{L}} = C_{\mathrm{L}}(\alpha, \hat{q}, \eta) - \frac{1}{2\alpha_{\mathrm{stall}}} C_{\mathrm{L}\alpha}\alpha^2 \tag{10}$$

such that the lift force decreases beyond stall.

4 Analysis

The flight envelope is characterised by the stable trim conditions such that the aircraft satisfies given constraints on the states and limitations on the control inputs. Here, we require $\gamma \in [-30°; 30°]$ and $\alpha \in [-3°; 12°]$, denoted by $\mathbf{x} \in \mathcal{C}$, as well as $\mathcal{U} = [-10°; 10°] \times [0; 125\,\mathrm{rev/s}]$. If the control authority is compromised, some trim conditions are unachievable, thus limiting the abilities of the drone to fly stably.

The nonlinear system of (1) is in a viable trim condition if

$$\mathbf{f}(\mathbf{x}^*, \mathbf{u}^*) = 0 \tag{11}$$

for $\mathbf{x}^* \in \mathcal{C}, \mathbf{u}^* \in \mathcal{U}$. A trim condition is further stable if and only if the Jacobian matrix,

$$\mathbf{J}^* = \frac{\partial \mathbf{f}}{\partial \mathbf{x}}(\mathbf{x}^*, \mathbf{u}^*)\,, \tag{12}$$

has only strictly negative eigenvalues. If, for some input $\mathbf{u}^*$, an eigenvalue of the Jacobian at the corresponding trim condition $(\mathbf{x}^*, \mathbf{u}^*)$ crosses zero and the trim condition changes stability, we have a critical point. For a single input parameter u, trim analysis is the result of a continuation method, where the equalities of $\mathbf{f}(\mathbf{x}, u^*) = 0$ are solved for small changes in u^* and stability of each trim condition is determined by $\mathbf{J}^*$. Continuation and bifurcation of a given system can be computed using mathematical toolboxes such as [16–18].

4.1 *Loss of propulsion*

Without a propulsion system, the aircraft is not able to input energy. That is, if the speed is to be constant, the altitude must decrease, thus exchanging potential for kinetic energy. In consequence, we expect a viable trim condition at zero thrust to have a negative inclination angle.

Fig. 2 shows the viable trim conditions in the event of loss of propulsion. The largest inclination is achieved for an elevator deflection $\eta \approx 2.8°$ with airspeed $V_\mathrm{A} \approx 7.7\,\mathrm{m/s}$. For larger deflections, the aircraft enters into a steeper descent thus speeding up; for negative deflections, however, angle of attack is increased until the trim condition becomes unstable and finally, the wing stalls ($V_\mathrm{stall} \approx 6.4\,\mathrm{m/s}$). With airspeed and inclination at stable trim condition given by the elevator deflection, we can compute the components of the velocity vector, that is, the horizontal and vertical speed. The relation of horizontal and vertical motion is illustrated in Fig. 3. Unsurprisingly, the steep descent provides high speeds in both components; whereas close to stall, the vertical descent is amplified with respect to the horizontal speed.

4.2 *Loss of elevator*

If the elevator surface is jammed, the aircraft looses authority over its main control surface of the longitudinal attitude. The position η_0 of the stuck surface now determines immediately the angle of attack at which the aircraft is trimmed. However, as the remaining throttle input enters the system in (2) and (3), there is still the possibility to control – and possibly stabilise – speed and inclination of the vehicle's path.

Trim conditions in the case of loss of elevator are shown by Fig. 4 for surface positions of $-1°$, $0°$, $1°$, and $1.5°$; the corresponding angles of attack are $9.0°$, $7.6°$, $6.3°$, and $5.6°$, respectively. Fig, 4 also shows the critical boundary, i.e., the boundary of stable trim conditions, which is a function of the position of the stuck elevator surface. The viable trim conditions are further limited by the necessity of a positive throttle command ($n \geq 0$), since there is no negative thrust. Inputs that prompt a stable trim condition are shown by Fig. 5. As we can obtain from this trim analysis, the MAKO aircraft is barely stable in case of an elevator jam in neutral position and neither for negative (pitching upwards) deflections. For increasingly positive deflections however, larger ranges of engine speed yield a stable trim.

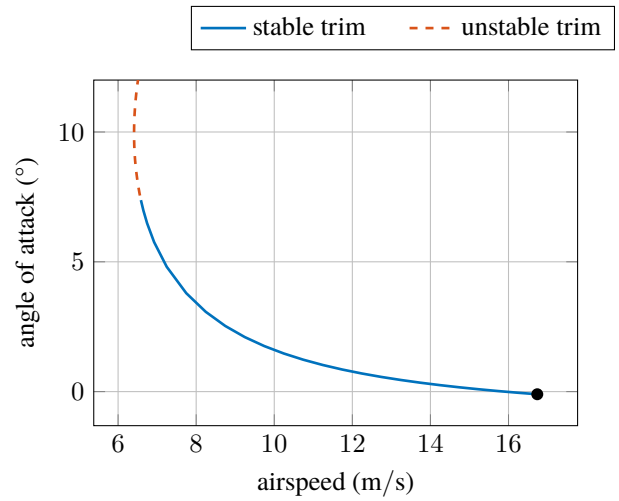

(a) Angle of attack α over airspeed V_A.

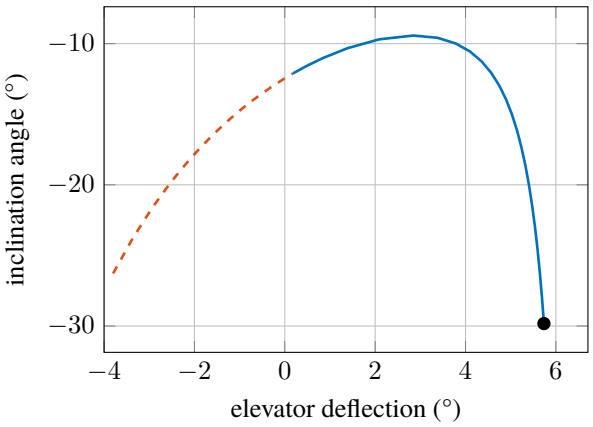

(b) Inclination γ over elevator deflection η.

Figure 2: Viable trim conditions in the event of loss of propulsion.

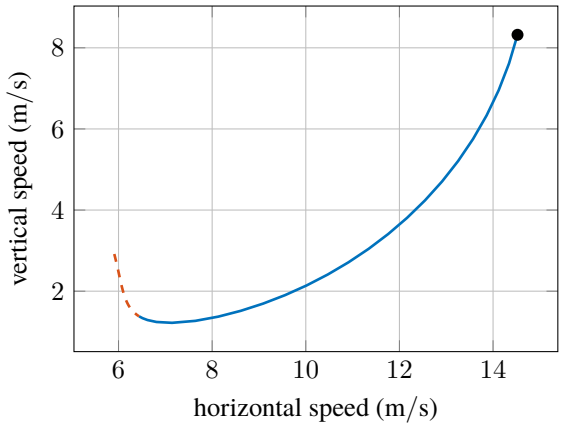

Figure 3: Composition of the velocity vector at trim condition in the event of loss of propulsion.

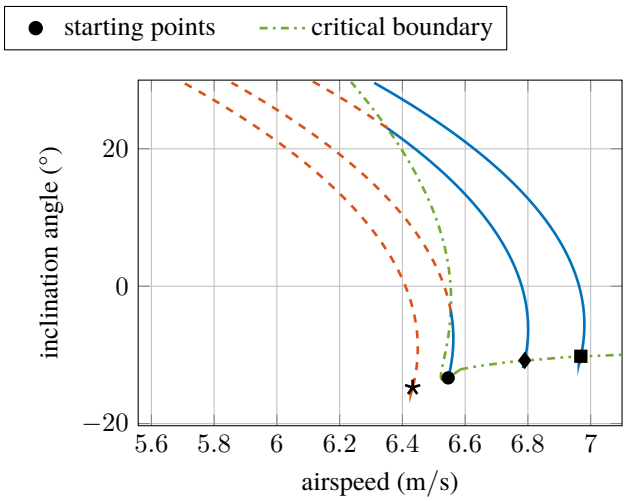

(a) Inclination γ over airspeed V_A.

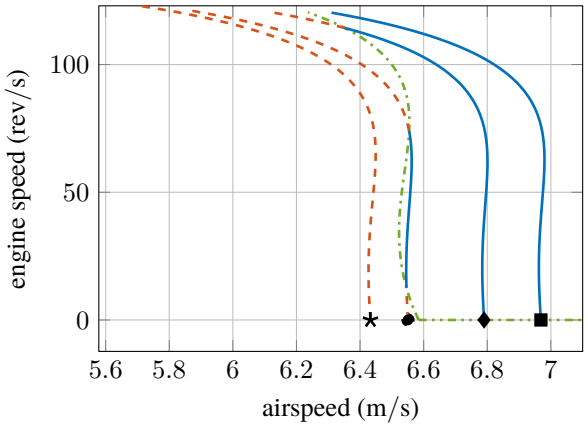

(b) Engine speed n over airspeed V_A.

Figure 4: Viable trim conditions in the event of loss of elevator. (Surface position: ⋆ $\eta_0 = -1°$; ● $\eta_0 = 0°$; ♦ $\eta_0 = 1°$; ■ $\eta_0 = 1.5°$.)

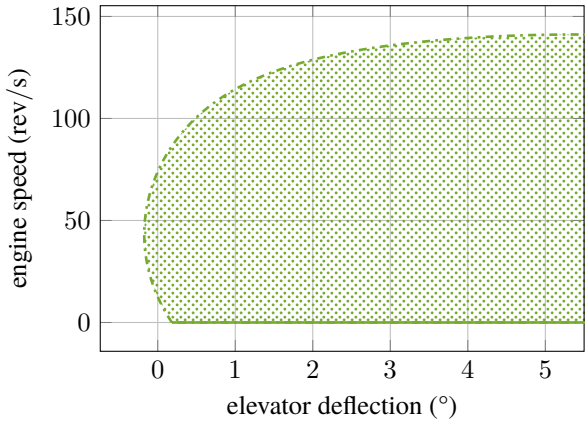

Figure 5: Stable inputs in the event of loss of elevator: engine speed n over surface position η_0.

4.3 *Loss of single aileron*

A single aileron jammed in no neutral position induces a roll moment onto the aircraft, making trimming without further relaxations difficult. If the second aileron can be deflected independently and to a symmetric – rather than anti-symmetric as usual – position equating the stuck surface, this cancels the roll moment and the discussion of trim conditions is similar to the previous case (for MAKO, where elevator and ailerons are combined into the elevon surface, we actually have the identical case). On the other hand, a relaxation on the trim constraints such as a nonzero roll rate might also lead to a deteriorated yet stable flight condition enabling a controlled descend.

A discussion of relaxed trim conditions requires an augmentation of the dynamic system with the lateral, six-degrees-of-freedom equations of motion as well as the continuation of limit cycles and is beyond the scope of this paper.

5 Landing Zones

If the aircraft cannot continue its mission due to an impairment, a suitable spot for landing or controlled flight into terrain is crucial in order to avoid further accidents. When discussing landing spots, we obvious have to take into account the vehicle's position in the earth-fixed reference frame; we thus extend the state vector to $\mathbf{y} = \begin{bmatrix}\mathbf{x} & \mathbf{x}_g\end{bmatrix}^T$ with

$$\dot{x}_g = V_A \cos\gamma_A \tag{13}$$
$$\dot{z}_g = -V_A \sin\gamma_A \tag{14}$$

representing the horizontal and vertical position. We denote the extended system dynamics by $\bar{\mathbf{f}}$ and have the constraints $\bar{\mathcal{C}} = \mathcal{C} \times \{\mathbf{x}_g \,|\, z_g \leq 0\}$. Given a certain aircraft state and position, we then have the set of *admissible landing spots* as

$$\mathcal{LS}[\mathbf{y}_0] = \{\mathbf{x}'_g | \exists \mathbf{x}' \in \mathcal{C}_L, \mathbf{y}(\cdot) \in \bar{\mathcal{C}}, \mathbf{u}(\cdot) \in \mathcal{U}, T > 0. \dot{\mathbf{y}} = \bar{\mathbf{f}}(\mathbf{y}, \mathbf{u}), \mathbf{y}(0) = \mathbf{y}_0, \mathbf{y}(T) = \begin{bmatrix}\mathbf{x}' & \mathbf{x}'_g\end{bmatrix}^T\} \cap \mathfrak{Surf}, \tag{15}$$

where $\mathcal{C}_L \subset \mathcal{C}$ are the landing conditions and $\mathfrak{Surf}$ is a model of the surface. For simplicity, we take $\mathfrak{Surf} = \{\mathbf{x}_g \,|\, z_g = 0\}$.

Solving (15) imposes an INF MIN optimal control problem. However, with some simplifications we can easily estimate bounds for a zone of controlled flight into terrain. Here, we relax the landing constraints to $\mathcal{C}_L = \mathcal{C}$ and further consider only trajectories where the aircraft is in trim condition almost all time. We further require that the set of stable, viable trim conditions is compact and connected.[2] Starting from the position difference

$$\Delta\mathbf{x}_g(\mathbf{y}_0, \mathbf{u}(\cdot)) = \int_0^T \dot{\mathbf{x}}_g(t)\,\mathrm{d}t \tag{16}$$

[2] We will argue that this requirement is given for the discussed events of loss-of-control.

with $\dot{\mathbf{y}} = \bar{\mathbf{f}}(\mathbf{y}, \mathbf{u})$ and $\mathbf{y}(0) = \mathbf{y}_0$, we approximate (16) as

$$\Delta\mathbf{x}_\mathrm{g}(\mathbf{y}_0, \mathbf{u}(\cdot)) \approx \int_0^T \dot{\mathbf{x}}_\mathrm{g}^*(t)\,\mathrm{d}t \tag{17}$$

with $\bar{\mathbf{f}}(\mathbf{y}^*, \mathbf{u}) = 0$ for almost all $0 \leq t \leq T$ and define the bounds

$$\overline{\Delta\mathbf{x}_\mathrm{g}} = T\dot{\mathbf{x}}_\mathrm{g}^*, \qquad \mathbf{f}(\mathbf{x}^*, \mathbf{u}_\mathrm{min}) = 0; \tag{18}$$

$$\underline{\Delta\mathbf{x}_\mathrm{g}} = T\dot{\mathbf{x}}_\mathrm{g}^*, \qquad \mathbf{f}(\mathbf{x}^*, \mathbf{u}_\mathrm{max}) = 0; \tag{19}$$

where $\mathbf{u}_\mathrm{min}$ ($\mathbf{u}_\mathrm{max}$) denote the respective control input such that there is a viable, stable trim condition with $\gamma_\mathrm{A} < 0$ and $|\gamma_\mathrm{A}|$ is minimal (maximal). We then have by boundedness of the interval (17)

$$\begin{aligned}\mathcal{CFT}[\mathbf{x}_{\mathrm{g}0}] = \big\{\mathbf{x}_\mathrm{g}' \big| \exists \mathbf{u} \in [\mathbf{u}_\mathrm{min}; \mathbf{u}_\mathrm{max}], T > 0.\\ \mathbf{x}_\mathrm{g}' - \mathbf{x}_{\mathrm{g}0} = T\dot{\mathbf{x}}_\mathrm{g}^*, \mathbf{f}(\mathbf{x}^*, \mathbf{u}) = 0\big\}\\ \cap\, \mathfrak{Surf}\end{aligned} \tag{20}$$

and obtain

$$\mathbf{x}_\mathrm{g} \in \mathcal{CFT}[\mathbf{x}_{\mathrm{g}0}] \Longleftrightarrow \frac{|x_\mathrm{g} - x_{\mathrm{g}0}|}{z_{\mathrm{g}0}} \in \left[\frac{\Delta x_\mathrm{g}}{\Delta z_\mathrm{g}}; \frac{\overline{\Delta x_\mathrm{g}}}{\overline{\Delta z_\mathrm{g}}}\right] \tag{21}$$

for $z_\mathrm{g} = 0$ if $\mathbf{x}_\mathrm{g} \in \mathfrak{Surf}$.

Landing without propulsion In the event of loss-of-propulsion, as we have seen in the section before, the aircraft has still a large range of stable yet descending trim conditions and the set of viable trim conditions is connected (Figs. 2 and 3). Therefore, the admissible zone of controlled flight into terrain depends mainly onto the initial height of the vehicle. Fig. 6 shows estimates for a linear approach and initial heights of 50 m, 150 m, and 250 m. Due to the fact that the aircraft is not able to descend vertically, there is not only a maximum reachability but also a minimal; clearly, the aircraft might also be able to reduce height in a descending turn, thus reducing the minimum distance for the (final) approach.

Landing with elevator jam Deprived of its mean of attitude control, the aircraft is in a severe state of fault; on the other, contrary to the case before, it still has the possibility to propel its flight – given sufficient battery or fuel. Whereas for the elevator jammed in neutral position there are only stable trim conditions with a descending path, for positive deflections the aircraft is too able to ascend stably (Fig. 4). In the latter case, the aircraft thus could, theoretically, stay aloft indefinitely: for instance, Fig. 7 illustrates the estimated admissible zones for controlled flight into terrain with elevator jams at deflections of 0°, 1°, 2°, and 5° (from quadrant I to IV). Note that a deflection of 5° without any throttle corresponds to fast and steep descent (see also Fig. 2) thus reducing the minimum approach distance with respect to the moderate deflections of 0° to 2°.

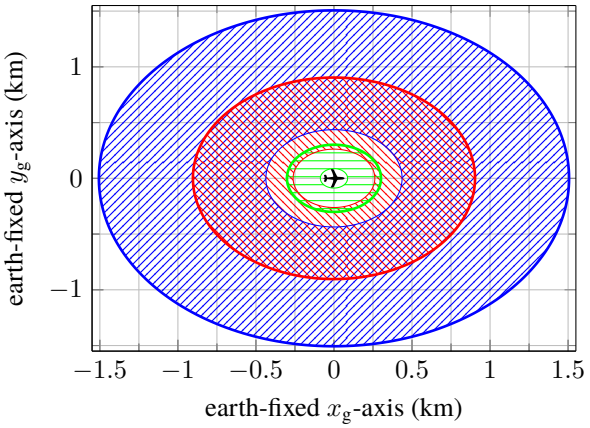

Figure 6: Estimated CFT zones for loss-of-propulsion. (Initial height: 50 m; 150 m; 250 m.)

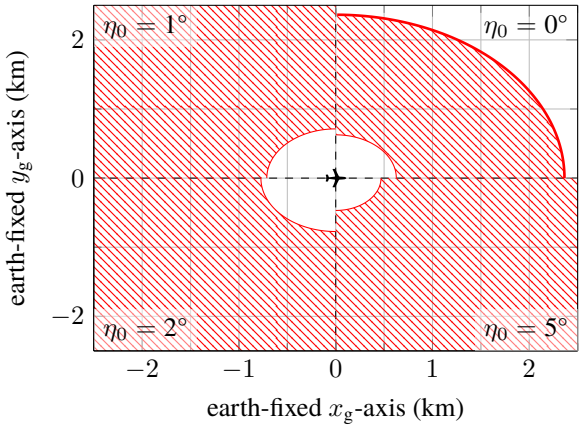

Figure 7: Estimated CFT zones for loss-of-elevator with initial height of 150 m ( ) and surface positions as indicated.

6 Conclusion

If a drone loses control authority over its inputs, stable flight conditions are often significantly restricted and continuation of flight might not be possible at all. In order to avoid LOC, information about flight abilities is crucial, as well as reachable zones for controlled flight into terrain. In this study, we discussed viable trim conditions of the longitudinal flight for the MAKO unmanned aircraft in the events of loss of propulsion or elevator. While, without thrust, the aircraft remains stable yet descends, for the elevator being jammed in pitch-up or neutral positions stable flight is (almost) impossible. Consequently, reachable landing spots are restricted both by the possible, minimal and maximal negative inclination angles. The proposed approach can be evaluated during design of the aircraft system.

References

[1] P. Russell and J. Pardee. Joint safety analysis team-CAST approved final report loss of control JSAT results

and analysis. Technical report, Commercial Aviation Safety Team, Washington, US-DC, 2000.

[2] Nathan D. Richards, Neha Gandhi, Alec J. Bateman, David H. Klyde, and Amanda K. Lampton. Vehicle upset detection and recovery for onboard guidance and control. *Journal of Guidance, Control, and Dynamics*, 40(4):920–933, 2016.

[3] *Loss of Control (LOC-I)*. European Aviation Safety Agency, Cologne, DE, 2018. URL https://www.easa.europa.eu/easa-and-you/general-aviation/flying-safely/loss-of-control#group-easa-downloads. (accessed August 20, 2018).

[4] Christine M. Belcastro, John V. Foster, Gautam H. Shah, Irene M. Gregory, David E. Cox, Dennis A. Crider, Loren Groff, Richard L. Newman, and David H. Klyde. Aircraft loss of control problem analysis and research toward a holistic solution. *Journal of Guidance, Control, and Dynamics*, 40(4):733–775, 2017.

[5] A. Lambregts, Gregg Nesemeier, Richard Newman, and James Wilborn. Airplane upsets: Old problem, new issues. In *AIAA Modeling and Simulation Technologies Conference and Exhibit*, page 6867, 2008.

[6] Guillaume J.J. Ducard. *Fault-tolerant flight control and guidance systems: Practical methods for small unmanned aerial vehicles*. Springer, Berlin, DE, 2009.

[7] Harry G Kwatny, Jean-Etienne T Dongmo, Bor-Chin Chang, Gaurav Bajpai, Murat Yasar, and Christine Belcastro. Nonlinear Analysis of Aircraft Loss of Control. *Journal of Guidance, Control, and Dynamics*, 36(1): 149–162, 2013.

[8] Stefan Schuet, Thomas Lombaerts, Diana Acosta, John Kaneshige, Kevin Wheeler, and Kimberlee Shish. Autonomous Flight Envelope Estimation for Loss-of-Control Prevention. *Journal of Guidance, Control, and Dynamics*, 40(4), 2017.

[9] Kevin McDonough and Ilya Kolmanovsky. Fast Computable Recoverable Sets and Their Use for Aircraft Loss-of-Control Handling. *Journal of Guidance, Control, and Dynamics*, 40(4):934–947, 2017.

[10] Robert C. Allen, Harry G. Kwatny, and Gaurav Bajpai. Safe Set Protection and Restoration for Unimpaired and Impaired Aircraft. In *AIAA Guidance, Navigation, and Control Conference*, Minneapolis, US-MN, 2012.

[11] H. N. Nabi, T. Lombaerts, Y. Zhang, E. van Kampen, Q. P. Chu, and Coen C. de Visser. Effects of Structural Failure on the Safe Flight Envelope of Aircraft. *Journal of Guidance, Control, and Dynamics*, 41(6):1257–1275, 2018.

[12] *Safe2Ditch Technology*. NASA Langley Research Center, Hampton, US-VA, 2018. URL https://technology.nasa.gov/patent/LAR-TOPS-243. (accessed August 22, 2018).

[13] Murat Bronz, Hector Garcia de Marina, and Gautier Hattenberger. In-flight thrust measurement using on-board force sensor. In *AIAA Atmospheric Flight Mechanics Conference*, page 0698, 2017.

[14] *Flight dynamics – Concepts, quantities and symbols – Part 1: Aircraft motion relative to the air*. International Organization for Standarization, Genève, CH, 4th edition, 1988.

[15] Murat Bronz. *A Contribution to the Design of Long Endurance Mini Unmanned Aerial Vehicles*. PhD thesis, Institut Supérieur de l'Aéronautique et de l'Espace, Toulouse, FR, 2012.

[16] Harry Dankowicz and Frank Schilder. *Recipes for Continuation*. Society for Industrial and Applied Mathematics, Philadelphia, US-PA, 2013.

[17] A. Dhooge, W. Govaerts, Yu. A. Kuznetsov, H. G.E. Meijer, and B. Sautois. New features of the software MatCont for bifurcation analysis of dynamical systems. *Mathematical and Computer Modelling of Dynamical Systems*, 14(2):147–175, 2008.

[18] Etienne Coetzee, Bernd Krauskopf, and Mark H Lowenberg. The Dynamical Systems Toolbox: Integrating AUTO into MATLAB. In *16th US National Congress on Theoretical and Applied Mechanics*, State College, US-PA, 2010.

Appendix A: Aerodynamic Coefficients

Coefficients for the aerodynamic and thrust model of MAKO are given by Tab. 2.

Table 2: Coefficients for the MAKO aircraft.

C_{L0}	-4.700×10^{-2}	–
$C_{L\alpha}$	3.944	–
C_{Lq}	4.820	–
$C_{L\eta}$	1.656×10^{-2}	–
C_{D0}	2.313×10^{-2}	–
C_{DL}	1.897×10^{-1}	–
C_{m0}	4.300×10^{-2}	–
$C_{m\alpha}$	-3.234×10^{-1}	–
C_{mq}	-1.683	–
$C_{m\eta}$	-7.600×10^{-3}	–
C_{F0}	1.342×10^{-1}	rev^{-2}
C_{FJ}	-1.975×10^{-1}	rev^{-1}
C_{Fn}	4.229×10^{-4}	$\mathrm{s\,rev}^{-3}$